Numerical Investigation of Blended and Raked Winglets Characteristics

MOHAMMED HUSSAIN FAROOK, VISHNU KUMAR G. C.
Department of Aeronautical Engineering
Hindustan Institute of Technology and Science
Chennai
INDIA

Abstract: - This research compares the efficiency of various winglet designs to reduce lift-induced drag by altering the amount and distribution of vortices at the wingtip and with changes to the baseline wing's aerodynamic properties. To explore the three-dimensional flow and vortex formation around the half wing, computational simulations utilizing the Reynolds Averaged Navier-Stokes equations and the K-SST turbulence model were run using Ansys Fluent R19.2. The simulation demonstrates that there is a significant correlation between the wing's lift, drag, and pitching moment, as well as the size of the tip vortex. The redesigned wing works distributes the vortices and minimizes drag. It was observed that optimizing the winglet tips was essential for increasing the lift coefficient while lowering the contributions of frictional and vortex drag components. It was observed that the lift increased with the winglet tips, the increase in frictional drag caused by the wetted surface area is a barrier to aerodynamic efficiency. The findings indicate that the chevron-type tips is best in reducing drag. It is outperformed by wings without chevron winglets in terms of lift-to-drag ratio. It is determined that chevron tips are the best winglet as their aerodynamic efficiency is essential for increasing flight range and endurance. Overall, it is observed that winglets are more efficient at lower aspect ratios and that a moderate aspect ratio of 10 offers the greatest increase in aerodynamic efficiency.

.

Key-Words: - Winglets, Blended type, Raked type, CFD, Vortices

Received: March 14, 2023. Revised: November 25, 2023. Accepted: December 27, 2023. Published: January 31, 2024.

1 Introduction

The Prandtl lifting line theory [1], states that the lift created by the wing can be estimated by integrating the circulation throughout the wing, to understand the three-dimensional lift distributions across a wing. Owing to the wing's finiteness, the circulation creates tip vortices, which are three-dimensional effects near the wingtips, as seen in Fig. 1. These vortices create lift-induced drag known as vortex drag. The lift-induced drag impacts the three-dimensional vortex flow around the wingtip region. Hence the winglets can stop the flow on the upper surface of the wing from flowing over it, which eliminates the wing tip vortices. As a result, the strength of wingtip vortices and the resulting lift-induced drag would be reduced. Nevertheless, the increase in aerodynamic efficiency brought about by the integration of such wing-tip devices largely depends on the wingtip design. Whitcomb [2] experimentally explored the aerodynamic effectiveness of a wing tip sail, to analyze the winglets to reduce the lift-induced drag. Many tip-device combinations have potential benefits; however, [3] studies that include all pertinent variables have not revealed any one configuration to have a clear overall advantage over the others. On par with changes that could result from the implementation of a modified few locations on the wingtip can be modified without having a significant effect on performance. In general, a raked tip extension will often be the most affordable choice. The impact of wingtip vortices can be considerably lessened with proper design. According to research [4], the two vortex cores that are created when the split winglets bend in low-pressure

areas may come together to form a single vortex. This lone vortex travels in a straight line behind the wing and interacts favorably with the other components of the fuselage, increasing the aircraft's range as shown in Figure 1.

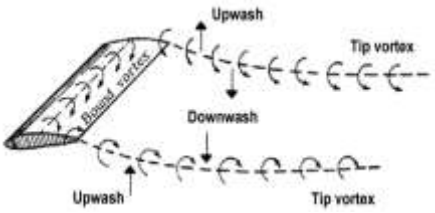

Figure 1: Formation of tip vortices due to secondary flows.

2 Problem Formulation

The commercial CFD tool Ansys Fluent 19.2 has been used to simulate the exterior flow aerodynamics numerically. Using a second-order centered difference technique for the diffusive terms, the variable values are interpolated at the face positions from their cell-centered values. A second-order upwind technique is used to interpolate the convective terms at cell faces. The least squares cell-based reconstruction approach is used to calculate the gradients at cell centers. The usage of a multi-dimensional gradient limiter prevents erroneous oscillations. The SIMPLE method is utilized to produce the pressure-velocity coupling, and the default under-relaxation settings were employed. The pressure checkerboard instability is avoided by using the Rhie-Chow interpolation approach since the solution occurs in collocated meshes. For the turbulence modeling, k – ω and SST model is used [5]. By resolving stable Reynolds averaged three-dimensional Navier Stokes equations, the current case's solution is sought. The Spalart Allmaras, k - ε, and k – ω and SST RANS CFD models were taken into consideration before the k - omega shear stress model was selected. This choice was taken after taking into account how well the K-omega model could depict the impacts of turbulence. This is because the higher-order stress relaxation terms were correctly predicted. The near-field viscous sublayer is precisely captured in the k – ω SST model developed [6, 7] by employing the more computationally intensive k - ε model in the region next to the wall. Nevertheless, it employs the k model, which utilizes comparatively fewer resources for far-field applications, allowing for greater flow resolution with the available computing resources. The two-equation model that was used in the current study's mathematical formulation is stated as,

Turbulence Kinetic Energy

$$\frac{\partial}{\partial t}(\rho k) + \frac{\partial}{\partial x_j}\left(\rho k u_j\right) = P - \beta^* \rho \omega k + \frac{\partial}{\partial x_j}\left[(\mu + \sigma_k \mu_t)\frac{\partial k}{\partial x_j}\right] \quad (1)$$

Specific Dissipation Rate

$$\frac{\partial}{\partial t}(\rho \omega) + \frac{\partial}{\partial x_j}\left(\rho \omega u_j\right) = \frac{\gamma}{\vartheta_t} P - \beta \rho \omega^2 k + \frac{\partial}{\partial x_j}\left[(\mu + \sigma_\omega \mu_t)\frac{\partial \omega}{\partial x_j}\right] + 2(1 - F_1)\sigma_{\omega^2}\frac{1}{\omega}\frac{\partial k}{\partial x_i}\frac{\partial \omega}{\partial x_i} \quad (2)$$

3 Methodology

The numerical analysis is performed using computational fluid dynamics (CFD) on two modified shapes of winglets: blended and raked. To determine the significance of a winglet, the results of these comparisons are made with wing without winglets. The Ansys Fluent Solver is used to do the CFD simulation for an angle of attack range of (0°- 16°) with 4° as increment for all models in low subsonic flow with Reynolds Number of 676796 at standard atmospheric condition.

3.1 Model design and Mesh generation:

To attain a high aspect ratio, a planar three-dimensional wing with a 3m span, 0.25 m chord at the root, and 0.2m chord at the wingtip and 0.15m height of the blended winglet was modelled using the NACA 2412 airfoil [8, 4]. The calculated wing area is 0.6 m^2. It should be mentioned that the majority of the studies in the winglet area used the same approach to design its geometry. The blended, raked, and modified winglets depicted in Figure 2 & 3 are attached to the baseline wing. The study's winglet span is equivalent to 20% of the baseline wing's wingspan by earlier research by many authors [2,10,11], who recommended using winglet span values between 10% and 20% of the wingspan. All the winglet heights have been maintained at 20% of the semi-wingspan for all cases as suggested by [9] for maximum efficiency. The NACA 2412 airfoil is used to simulate each winglet and its tip while preserving a zero-toe angle about the incoming flow.

Figure2.a) Conventional wing Figure b) Raked winglet 25^0 [12].

Figure 3 a) Blended winglet 30^0 b) Raked winglet with chevron.

Tetrahedral elements are taken into account while creating the mesh for the current computational domain, which is refined from a The initial coarse mesh of 0.15 million elements is varied to a final mesh of 2 million elements..

The solution was iterated and the mesh was refined based on a grid-independent analysis until all the forces were fully captured and there was no increase in convergence with additional mesh refinement. It has been noted that domains with 1.6 million or more elements only modify the drag coefficient at the fourth decimal place. As a result, the converged grid for the current investigation was chosen from a domain with 2.0 million cell components. Several wing geometries also underwent the same type of mesh independent testing as shown in figure 4.

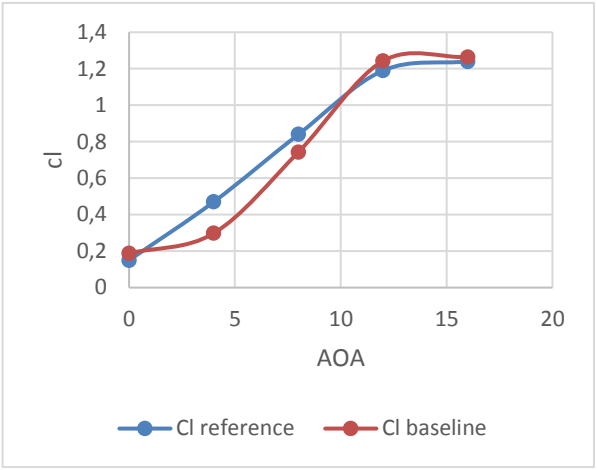

Figure 4: validation of conventional wing [4]

4 Results and Discussion

The computational domain's boundaries are increased by six times the dimensions of the model. The exterior wing surface is handled as a no-slip fixed wall. The enclosure's edges are regarded as walls with no shear. The inlet velocity of 40 m/s, is given to the normal boundary of the flow domain in front of the leading edge of the aircraft wing. To account for low-altitude flying regimes that would render the wing more susceptible to stalling, a turbulence intensity of 5% was chosen at STP. External air pressure is set to zero-gauge pressure at the flow domain's exit.

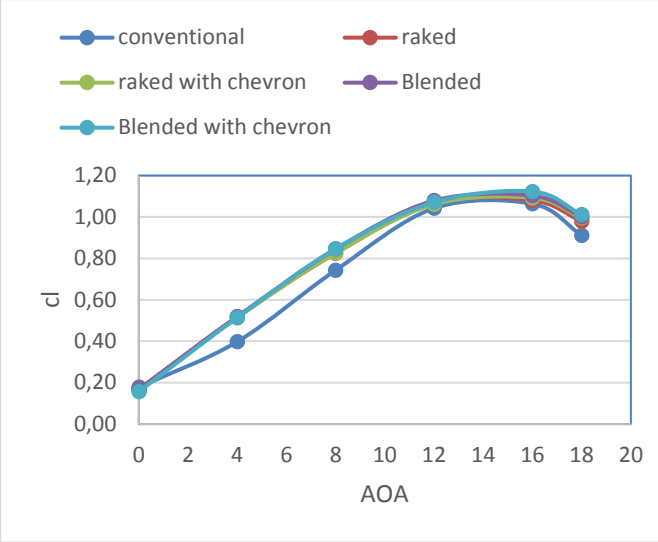

Figure 5: Cl Vs AOA

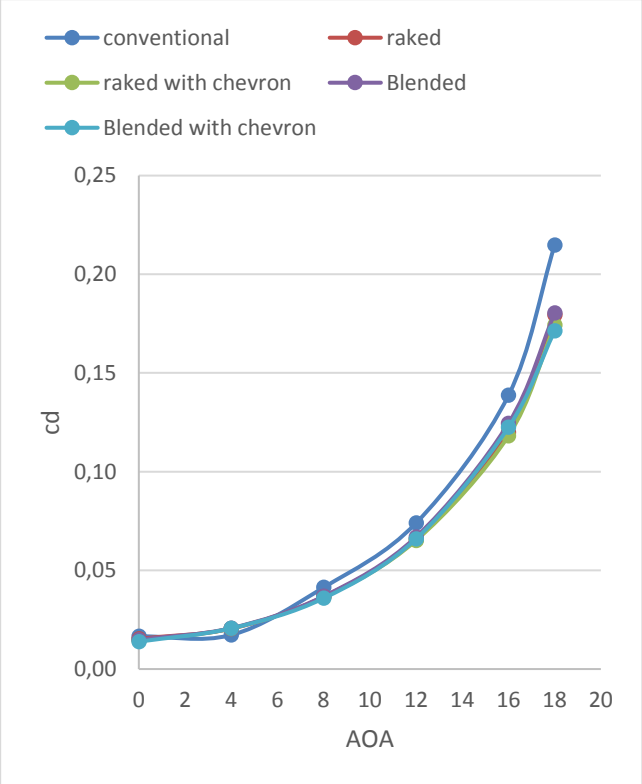

Figure 6: Cd Vs AOA

The blended chevron type provides a higher lift coefficient at a lower angle of attack conditions as shown in figure 5. Hence during the takeoff and landing conditions, the winglets are beneficial. The drag coefficient is also reduced for the blended with chevron-type winglets compared to conventional type as shown in figure 6. The Pressure and velocity contours are shown in Figure 7.

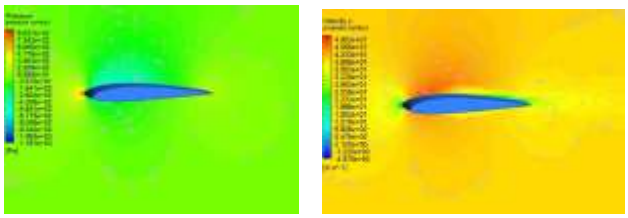

Figure 7. Pressure and velocity contours of conventional wing without winglets at 40m/s.

5 Conclusion

The wingtip modifications on the conventional wing lead to significant changes in the aerodynamic characteristics. The blended wing with chevron modification results in an increase of lift/ drag ratio compared to the blended and raked type winglets. Further modification in changing the ratio of different chevron types will be analyzed further.

References:

[1] J.D. Anderson, Fundamentals of Aerodynamics, McGraw-Hill, New York, 2011.
[2] R.T. Whitcomb, A design approach and selected wind-tunnel results at high subsonic speeds for wing-tip mounted winglets, NASA TN D-8260, NASA Langley Research Centre, 1976.
[3] [3] D. McLean, “Wingtip Devices: What They Do and How They Do It,” Boeing Perform. Flight Oper. Eng. Conf., Boeing, Article 4, 2005.
[4] Gautham Narayan, Bibin John, 2016, Effect of winglets induced tip vortex structure on the performance of subsonic wings, 10.1016/j.ast.2016.08.031, Aerospace Science and Technology, September 2016, 2020-05-11.
[5] Wilcox, D.C. Turbulence Modeling for CFD; DCW Industries: La Cañada Flintridge, CA, USA, 2010.
[6] F. R. Menter, “Zonal Two Equation k-ω Turbulence Models for Aerodynamic Flows,” American Institute of Aeronautics and Astronautics, Inc., Reston, 1993.
[7] F. R. Menter, Two-Equation Eddy-Viscosity Turbulence Models for Engineering Applications, AIAA Journal, vol. 32, no 8. pp. 1598-1605, 1994.
[8] Abbott, Ira H., Albert E. von Doenhoff, and Louis Stivers Jr. Theory of Wing Sections, Including a Summary of Airfoil Data. (1945).
[9] Jason E. Hicken and David W. Zingg, Induced-Drag Minimization of Nonplanar Geometries Based on the Euler Equations, AIAA Journal Vol. 48, No. 11, November 2.

[10] Shollenberger, C.A. Application of an Optimized Winglet Configuration to an Advanced Commercial Transport; Technical Report NASA-CR-159156; NASA: Washington, DC, USA, 1979.
[11] Smith, L.; Campbell, R. Effects of Winglets on the Drag of a Low-Aspect-Ratio Configuration; Technical Report NASA-TP-3563; NASA: Washington, DC, USA, 1996.
[12] Joel H, Daniel P, Thomas Y, Aerodynamic Optimization and Evaluation of KC-135R Winglets, Raked Wingtips, and a Wingspan Extension; 48th AIAA Aerospace Sciences Meeting Including the New Horizons Forum and Aerospace Exposition; 10.2514/6.2010-57.

Contribution of Individual Authors to the Creation of a Scientific Article (Ghostwriting Policy)

The authors equally contributed in the present research, at all stages from the formulation of the problem to the final findings and solution.

Sources of Funding for Research Presented in a Scientific Article or Scientific Article Itself

No funding was received for conducting this study.

Conflict of Interest

The authors have no conflicts of interest to declare that are relevant to the content of this article.